MINNEAPOLIS • MAY 20-24, 2018

Investigation of Foil Journal Bearing Performance by Generalized Differential Quadrature (GDQ) Method

M. Mehdizadeh[1], B. Hajshirmohammadi[1], A. Ghobadi[2], M. Esfahanian[3]
[1]Department of Mechanical and Industrial Engineering, Louisiana State University, USA
[2]Department of Mechanical Engineering, Islamic Azad University of Khomeini-Shahr, Iran
[3]Department of mechanical engineering, Isfahan University of Technology, Isfahan, Iran

INTRODUCTION

Many research has been conducted on wear mechanisms and tribology behavior of materials and components such as gear, bearings, etc [1-3]. Compliant journal bearings popularly known as foil bearings have gained significant attention in recent years because of their unique mode of operation and diversity of applications. These types of bearings have various advantages compared to the conventional rigid journal bearings in terms of higher load carrying capacity, lower power loss, better stability and greater endurance. These bearings are self-acting, and can operate with ambient air or any process gas as the lubricating fluid. The need for complex lubrication systems is eliminated, which result in significant weight reduction and lower maintenance. Air as a lubricant is available abundantly and can operate at elevated temperatures whereas conventional oil-based lubricants fail since their viscosity drops exponentially with the rise in temperature.
Figure (1) represents the configuration of a foil journal bearing. It is comprised of an outer bearing sleeve which houses the corrugated series of bumps on a thin foil strip and over the bump foil strip a thin smooth top foil sheet is laid. These foils are welded at leading edge and are free at the trailing edge.

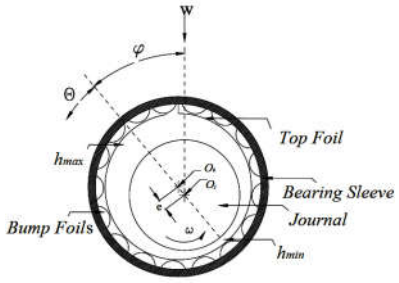

Fig. 1 Schematic of Compliant Journal Bearing

The series of bumps in the strip supports the top foil sheet and acts as a spring bed which makes the bearing compliant (Fig 2). The journal and bearing system are supported by a thin lubricant film (gas) due to the hydrodynamic pressure Distribution.

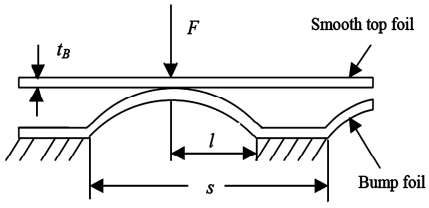

Fig. 2 Schematic Configuration of Top and Bump Foils

Blok and VanRossum (1953) first introduced the technical community to foil bearings and investigated a tension type CFB with analytical and experimental method [4]. Foil air bearings were first commercialized in the 1970s in air cycle machines used for

aircraft cabin pressurization [5]. Experimental and theoretical investigations show that foil bearings also offer better stability compared to the conventional rigid gas bearings [6].

Walowit and Anno first presented an elastic model for a single bump [7]. It was a two-dimensional model in which the bending and tensile stiffness of a bump was considered. This structural model was used by Heshmat et al. in an investigation of the steady state behavior of a foil bearing [8]. In their investigation, deflection of the foil structure was simplified with the assumption that the deflection was proportional to the pressure distribution. Heshmat and Ku showed that compliant journal bearings are able to handle greater loads with improvements in the compliant support structures [9]. Heshmat [10] first proposed a double-bump AFB[1], in order to improve the load capacity, damping [11-13], and stability. He successfully demonstrated the advances in performance at high load condition.

Dellacorte and Valco [14] classified the single-bump AFB as a first-generation bearing and the double-bump AFB as a third-generation bearing with a higher load capacity. The new set of equations were solved numerically and compared with numerical simulations using a finite approximation (Peng and Khonsari, 2004) for rigid bearings and compliant bearings [15]. Reddy was performed first considerable numerical analysis by using approximation method as Infinite Long bearing Approximate (ILA), Finite Element Method (FEM), and Modified Parabolic Approximate (MPA) [16].

The aim of this study is to focus on the modeling and simulation of foil journal bearings with consideration of the elastic behavior of the foil and gas compressibility. To predict the bearing performance parameters, the compressible Reynolds equation is solved based on Generalized Differential Quadrature Method (GDQM). The GDQ method reduces the classical Reynolds equation to algebraic linear system equations.

Appropriate equations and numerical solution are developed for treating a compressible Reynolds equation using GDQM. A numerical procedure is developed for predicting the foil deformation, operating film thickness and load-carrying capacity of foil journal bearings over a large range of operating speeds. The lubricant used is air whose properties are indicated in Table 1 [17] and also the properties of foil are indicated in Table 2 [17]. It is worth mentioning that the operating speed is 30,000 rpm.

Viscosity (μ)	**184.6×10-7 N.s/m2**
Density (ρ0)	1.1614 kg/m3

Table 1: Lubricant Properties (Air)

Radius of Shaft (*R*)	**19.05×10-3m**
Bearing Length (*L*)	38.1×10-3m
Nominal Radial Clearance (*C*)	50×10-6m
Top Foil Thickness (t_t)	0.1016×10-3m
Bump Foil Thickness (t_b)	0.1016×10-3m
Bump Pitch (*s*)	4.572×10-3m
Bump Length (2*l*)	3.556×10-3m
Bump Foil Youngs Modulus (*E*)	200 ×109 Pa
Bump Foil Poisson's Ratio (ν)	0.31

Table 2: Generation 1 Compliant Bearing Data

The governing equation for pressure distribution with the ideal gas flow in a journal foil bearing is given by the Reynolds equation. The standard Reynolds equation is considered by neglecting the time variant.

$$\frac{\partial}{\partial x}\left(\frac{\rho h^3}{\eta}\frac{\partial p}{\partial x}\right)+\frac{\partial}{\partial y}\left(\frac{\rho h^3}{\eta}\frac{\partial p}{\partial y}\right)=12\tilde{u}\frac{\partial(\rho h)}{\partial x}+12\tilde{v}\frac{\partial(\rho h)}{\partial y} \quad (1)$$

For ideal gas:

$$p=\rho \bar{R} t_m \quad (2)$$

The Reynolds equation of incompressible lubrication in nondimensional form is written as [18]:

[1] Air Foil Bearing

$$L(\psi)=(\psi+h^{\frac{3}{2}})\left(\frac{\partial^2\psi}{\partial x^2}+\alpha^2\frac{\partial^2\psi}{\partial y^2}\right)+\left(\frac{\partial\psi}{\partial x}\right)^2$$
$$+\alpha^2\left(\frac{\partial\psi}{\partial y}\right)^2-\frac{3}{2}\frac{dh}{dx}\psi\frac{\partial\psi}{\partial x}+\frac{3}{2h^2}\left[(\frac{dh}{dx})^2-h\frac{d^2h}{dx^2}\right]\psi^2$$
$$-\frac{3}{4}\frac{1}{\sqrt{n}}\left[(\frac{dh}{dx})^2-2h\frac{d^2h}{dx^2}\right]\psi \qquad (3)$$
$$-\beta\left(\frac{1}{\sqrt{n}}\frac{\partial\psi}{\partial x}-\frac{1}{\frac{3}{2h^2}}\frac{dh}{dx}\psi-\frac{dh}{dx}\right)=0$$

$$\alpha=\frac{\pi}{\lambda},\quad \beta=2\pi\Lambda,\quad \Lambda=\frac{6\bar{\mu}\bar{U}\bar{R}}{\bar{P}_a\bar{C}^2} \qquad (4)$$

where Λ represents the compressibility number or the bearing number.

Although the GDQ method may well be applied to multidimensional problems with physical domains of irregular geometry [19], the following discussion is confined to a square domain $0\le x\le 1$, $0\le y\le 1$, for convenience and due to its suitability to the present problem. The very basis of the differential quadrature method (DQM) rests on approximating the partial derivatives of a function with respect to a coordinate direction at any discrete point as the weighted sums of the values of the function at all the discrete points chosen in that direction. Thus, nth order partial derivatives of a field variable $\psi=\psi(x,y)$ may be written as:

$$\left.\frac{d^n\psi}{dx^n}\right|_{x_i}=\sum_{j=1}^{N_x}C_{ij}^{xn}\psi\left(x_j,y\right);\ \ for\ i=1,2,...,N_x\ ;\ 0<x<1 \qquad (5)$$

Where N_x is the number of discrete or sampling points in the x-direction of the field variable domain and C_{ij}^{xn} are the weight-in coefficients associated with nth order partial derivative with respect to x at the discrete point x_j. . If m=1, namely, for the first order derivative.

$$C_{ij}^{1}=\frac{M^{(1)}\left(x_i\right)}{\left(x_i-x_j\right)M^{(1)}\left(x_j\right)} \qquad (6)$$
$$i\ne j, i=j=1,2,..,N$$

$$C_{ii}^{1}=-\sum_{j=1,j\ne i}^{N}C_{ij}^{1}\ \ ,i=1,2,...,N \qquad (7)$$

In order to determine the weighting coefficients, the field variable needs to be approximated with some test function; the only requirements of the test functions being those of smoothness and differentiability at least to the highest order derivative in the differential equation. $M^1(x)$ is the first derivative of *M(x)* and they can be defined as:

$$M\left(x\right)=\left(x-x_1\right)\left(x-x_2\right)..\left(x-x_N\right) \qquad (8)$$
$$M^{1}\left(x_i\right)=\prod_{k=1,k\ne i}^{N}\left(x_i-x_k\right)$$

$$C_{ij}^{(m)}=m\left(C_{ij}^{1}C_{ij}^{(m-1)}-\frac{C_{ij}^{(m-1)}}{x_i-x_j}\right) \qquad (9)$$
$$i\ne j, i,j=1,2,...,N;\ \ m=2,3,...,N-1$$

$$C_{ii}^{m}=-\sum_{j=1,j\ne i}^{N}C_{ij}^{m}\ \ ,i=1,2,...,N \qquad (10)$$

The present coordinate distribution of discrete grid points can be chosen arbitrarily. In this work, the intermediate sampling points between x=0 and x=1 are taken from the first order zeros of shifted chebyshev polynomials for polynomial test function.

$$x_1 = 0, x_i = \frac{1}{2}\left[1 - \cos\left(\frac{(2i-1)\pi}{2N}\right)\right] \tag{11}$$

$$x_i = \frac{i-1}{N-1}, \qquad i = 1,2,\ldots,N$$

In analogy to the classical quadrature case [19] , the test functions are chosen of the form:

$$\psi_k(x,y) = x^{k-1}Y(y) \;; k = 1,2,...,N_x \tag{12}$$

Harmonic Test Functions

Due to the fitting exactness of a polynomial of order AA - 1 to the *N* sampling points, the choice of a polynomial test function seems to be most suitable wherever it can be used. However, there can be situations where a polynomial may be entirely unsuitable. One such case is when the field variable *\l/(x, y)* is periodic in one or more coordinate directions. Assuming the test function to be periodic in the x-direction, an appropriate choice of the test functions in the x-direction would be [20]:

$$\begin{aligned} \psi_k(x, y) &= \cos\left[2(k-1)\pi\right] \times Y(y) \\ &\quad ; k = 1,2,...,(N_x/2) + 1 \\ \psi_k(x, y) &= \sin\left[2\left(k - \frac{N_x}{2} - 1\right)\pi x\right] \times Y(y) \\ &\quad ; k = (N_x/2) + 2,(N_x/2) + 3,..., N_x \end{aligned} \tag{13}$$

Application of GDQM to governing equation

Equation (24) is a nonlinear differential equation and its Solution is obtained via Newton's method [21, 22]. Accordingly, first, the iterative process of Newton's method is defined as:

$$\psi^{(n+1)} = \psi^{(n)} + \eta^{(n)} \tag{14}$$

where *n* is the iteration count and the correction η is obtained from the solution of the equation written in the operator form as:

$$\eta^{(n)} L'(\psi^{(n)}) + L\psi^{(n)} = 0 \tag{15}$$

In Eq. (15), *L(ψ)* is the left-hand side of the Reynolds equation, Eq. (3), and *L′(ψ)* is the Frechet derivative of *L(ψ)* defined as:

$$\eta L'(\psi) = \frac{\partial}{\partial \Delta} + L(\psi + \Delta\eta)\,|_{\Delta=0} \tag{16}$$

On substituting Eq. (3) and the Frechet derivative from Eq. (16) in Eq. (15), one may see that the correction η is governed by the following linear differential equation

$$\begin{aligned} &(\psi + h^{\frac{3}{2}})\left(\frac{\partial^2\eta}{\partial x^2} + \alpha^2\frac{\partial^2\eta}{\partial y^2}\right) + \left(2\frac{\partial\psi}{\partial x} - \frac{3}{h}\frac{dh}{dx}\psi - \frac{\beta}{\sqrt{n}}\right)\frac{\partial\eta}{\partial x} \\ &+ 2\alpha^2\frac{\partial\psi}{\partial y}\frac{\partial\eta}{\partial y} + \left[\frac{\partial^2\psi}{\partial x^2} + \alpha^2\frac{\partial^2\psi}{\partial y^2} - \frac{3}{h}\frac{dh}{dx}\frac{\partial\psi}{\partial x}\right]\eta + \\ &\left[\frac{3}{h^2}\left\{\left(\frac{dh}{dx}\right)^2 - h\frac{d^2h}{dx^2}\right\}\psi\right]\eta + \\ &\left[-\frac{3}{4}\frac{1}{\sqrt{h}}\left\{\left(\frac{dh}{dx}\right)^2 - 2h\frac{d^2h}{dx^2}\right\} + \frac{\beta}{2h^{\frac{3}{2}}}\frac{dh}{dx}\right]\eta + L(\psi) = 0 \end{aligned} \tag{17}$$

where the superscript *(n)* is omitted for convenience. Now applying differential quadrature to Eq. (17), one obtains:

$$
\begin{aligned}
&(\psi_{ij} + h_i^{\frac{3}{2}})(\sum_{K=1}^{N_X} A_{ik}^{xx}\eta_{kj} + \alpha^2 \sum_{K=1}^{N_y} A_{jk}^{xx}\eta_{ik}) + \\
&\left(2\frac{\partial\psi}{\partial x} - \frac{3}{h}\frac{dh}{dx}\psi - \frac{\beta}{\sqrt{n}}\right)\sum_{K=1}^{N_X} A_{ik}^{x}\eta_{kj} + \\
&2\alpha^2\left(\frac{\partial\psi}{\partial x}\right)_{ij}\sum_{K=1}^{N_y} A_{jk}^{y}\eta_{ik} + \left[\frac{\partial^2\psi}{\partial x^2} + \alpha^2\frac{\partial^2\psi}{\partial y^2} - \frac{3}{h}\frac{dh}{dx}\right]_{ij} + \\
&\left[\frac{3}{h^2}\left\{\left(\frac{dh}{dx}\right)^2 - 2h\frac{d^2h}{dx^2}\right\} + \frac{\beta}{2h^{\frac{3}{2}}}\frac{dh}{dx}\right]_{ij} \\
&= -[L(\psi)]_{ij} \quad i = 1,2,...,N_x\,;\, j = 1,2,...,N_y
\end{aligned}
\tag{18}
$$

where i and j refer to a point (x_i, y_j) in the mesh shown in Fig (3).

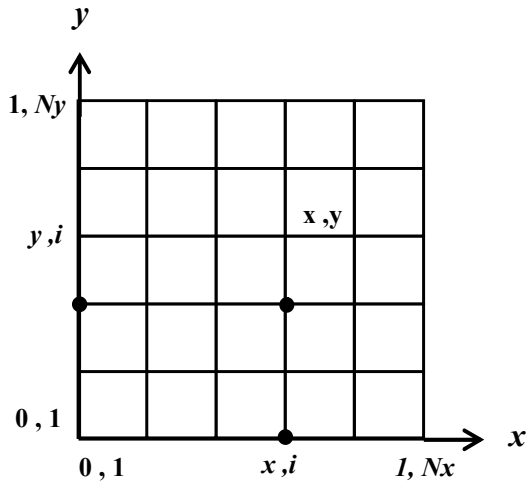

Fig. 3 Mesh for differential quadrature solution

For a rigid gas bearing, the functional form of the Non-dimensional film thickness is represented as:

$$\bar{h}_r = 1 + \varepsilon_r \cos\theta \tag{19}$$

But in case of a foil bearing, since the bushing is compliant, the film thickness is a function of the pressure.

$$\bar{h}f = 1 + \varepsilon_f \cos\theta + \alpha(\bar{p} - 1) \tag{20}$$

$$\bar{h} = \frac{h}{C}\ , \quad \varepsilon = \frac{e}{C}\ , \qquad \bar{p} = \frac{p}{p_a}\ , \quad \alpha = \frac{2p_a s}{CE}(\frac{L}{t})^2(1-\nu^2) \tag{21}$$

Where α represents the compliance number. Note that in Eq. (20) the eccentricity ratio (ε_f) can be greater than one while maintaining a positive minimum film thickness. This is so because as the pressure deforms the top foil, it enlarges the original clearance, providing additional room for the shaft to move towards the minimum film thickness, $h_{\min}$. The arithmetic mean pressure in the axial direction is used to calculate the top foil deformation and that the film thickness using Eq-20.

The solution of Reynolds equation begins by GDQM by an initial guess pressure p_{ij}^n, by solving for an incompressible bearing with an assumed rigid bearing eccentricity ratio ε_r and an initial guess for the film thickness $\overline{h_{i,j}}$, This is done iteratively until a convergence of the pressure is achieved for a given film thickness. Convergence of film thickness is assumed when the relative error of film thickness between two successive iterations falls below a tolerance value of 0.1 percent. The next part is to couple the hydrodynamic

pressure and the foil structural compliance which has a direct effect on the overall behavior of the fluid film profile. This is incorporated in an iterative scheme.
Therefore, once the deformation of top foil is taken into account, the eccentricity and the attitude angle must be modified in order to analyze the overall change in the film thickness. The numerical procedure adapted for modifying the film thickness in an iteration scheme is shown below.

$$\bar{h}^{n+1}_{f_{i,j}} = 1 + \varepsilon^{n}_{f} \cos\theta + \alpha(\bar{p}^{n}_{i,j} - 1) \tag{22}$$

$$\varepsilon_{f} = \varepsilon_{r} + \Delta\varepsilon \tag{23}$$

Where $\Delta\varepsilon$ is the change of eccentricity ratio due to the deformation of top foil and $\Delta\varphi$ is the change of attitude angle and n is the iteration number. The foil bearing eccentricity is described by the following relationship. The boundary conditions of the correction variable η are:

$$\psi(x, y) = \psi(x + 1, y) \qquad \textit{periocity condition} \tag{24}$$

$$\psi(x,0) = \psi(x,1) = 0 \quad \textit{bearing ends open to the ambient} \tag{25}$$

Results and discussion

In order to assess the advantages of the differential quadrature method, the foremost requirement is to look into the accuracy of its numerical computations vis-a-vis the available results in the literature. However, in the case of journal bearings with incompressible lubrication, harmonic test functions were used in the circumferential direction with polynomial test functions in the y-direction. Also, either with incompressible or compressible lubrication, intermediate sampling points for polynomial test functions were taken as the zeros of the shifted Chebyshev polynomials while, for the harmonic test functions, the sampling points were obtained from Eq. (12).
In journal bearings with compressible lubrication, a continuous (gas) film exists all over the journal without any breakup and, consequently, the pressure or ψ-function and the correction variable η need to be continuous periodic functions in the circumferential direction (see Eqs. (13)). Therefore, in the case of journal bearings with compressible lubrication, use of harmonic test functions was necessary for the circumferential (x) direction. However, in the case of journal bearings with incompressible lubrication, the lubricant film does not happen to be continuous due to cavitation and, therefore, unlike in the case of compressible lubrication, the pressure is not a continuous periodic function in the circumferential direction. Thus, in the case of journal bearings with incompressible lubrication, harmonic test functions are really not applicable.
The effectiveness of the method may be seen from the fact that beginning with the approximation $\psi = 0$, the solution converges in no more than three or four iterations even for eccentricities near unity and very high compressibility numbers. In fact, in any case, the solution always converges in two or three iterations if initial guess values of ψ are taken as the values established for some nearby parameters (λ, ε, and/or Λ). The following criterion was applied for terminating the iterations of Newton's method:

$$\frac{\sum_{i=1}^{N_x}\sum_{j=1}^{N_y} \eta_{ij}^{2}}{\sum_{i=1}^{N_x}\sum_{j=1}^{N_y} \psi_{ij}^{2}} \le 10^{-5} \tag{26}$$

The results presented thus far establish quite conclusively that the generalized differential quadrature method is an accurate numerical technique for the solution of lubrication problems.

Load Carrying Capacity and attitude angle

Once the dimensionless pressure profile is obtained, the load-carrying capacity can then be calculated [18]. The x and z components In dimensionless form are:

$$w_x = -\pi \int_0^1 \int_0^1 \bar{p} \sin\theta \, dx \, dy = \pi \sum_{i=1}^{N_x}\sum_{j=1}^{N_y} C_i^x C_j^y \frac{\sin(2\pi x_i)\psi_{ij}}{\bar{h}_i^{\frac{3}{2}}} \tag{27}$$

$$w_z = \pi \int_0^1 \int_0^1 \bar{p} \cos\theta \, dx \, dy$$
$$= \pi \sum_{i=1}^{N_x} \sum_{j=1}^{N_y} C_i^x C_j^y \frac{\cos(2\pi x_i)\psi_{ij}}{\bar{h}_i^{\frac{3}{2}}} \quad (28)$$

The total dimensionless load is:

$$w = \sqrt{w_x + w_z} \quad (29)$$

Table 3 presents the load carrying capacity and attitude angle for the foil bearing by FDM [45] and GDQM.

ε_r		FDM [14]			GDQ (Present Work)		
	N_X* N_Y	ε_f	W_r	W_f	ε_f	W_r	W_f
0.3	50*10	0.3231	11.844	11.943	0.326548	13.818754	**13.877233**
0.3	100*20	0.3261	13.615	13.665			
0.3	120*20	0.3279	13.818	13.8722			
0.7	50*10	0.8727	69.027	72.1681	0.877592	71.489791	**73.595793**
0.7	100*20	0.8759	71.259	73.3726			
0.7	**120*20**	**0.8767**	**71.467**	**73.5969**			

Table 3 - Comparison of load capacity for a foil journal bearing, ε_r =0.1; N_x =12, $N_{y=8}$

ε_r		FDM [14]			GDQ (Present Work)		
	N_X* N_Y	ε_f	φ_r	φ_f	ε_f	φ_r	φ_f
0.3	50*10	0.3231	68.4325	68.3021	0.326548	70.476857	**70.397858**
0.3	100*20	0.3261	70.3127	70.2733			
0.3	120*20	0.3279	70.4771	70.3979			
0.7	50*10	0.8727	41.8896	39.6024	0.877592	42.753241	**40.849974**
0.7	100*20	0.8759	42.6598	39.9248			
0.7	**120*20**	**0.8767**	**42.7529**	**40.8498**			

Table 4 - Comparison of attitude angle for a foil journal bearing, ε_r =0.1; N_x =12, $N_{y=8}$

The results of the prediction on the load-carrying capacity of a foil bearing as a function of the bearing number for different L/D ratio is shown in Fig. 4 (a). Figure 4(b) is plotted to show the operating attitude angle of a foil gas bearing versus bearing number for different L/D ratio. The attitude angle comparison (Fig. 5(a)) revealed a comparable agreement for FDM and GDQM. Fig 5(b) represents the load comparison between the FDM and the GDQM for a range of eccentricity ratios. Since the main condition here was based on matching the minimum film, the load capacity varies slightly at higher eccentricity ratios. In the Fig. 5(c) load capacity for rigid and foil bearing have been plotted.

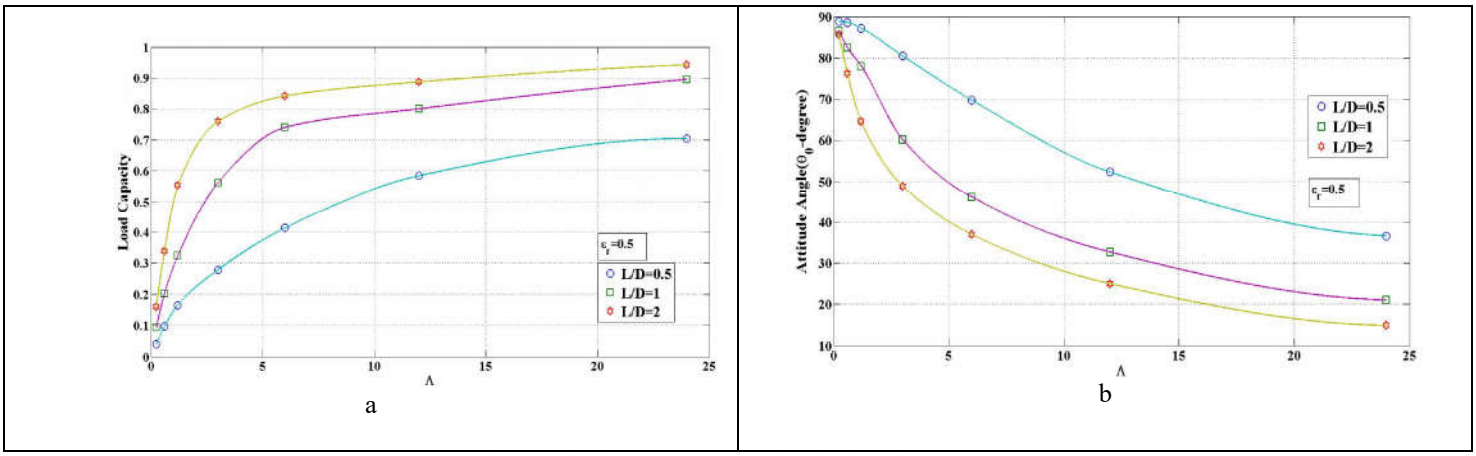

Fig. 4-(a) load support versus Λ (b) attitude angle versus Λ

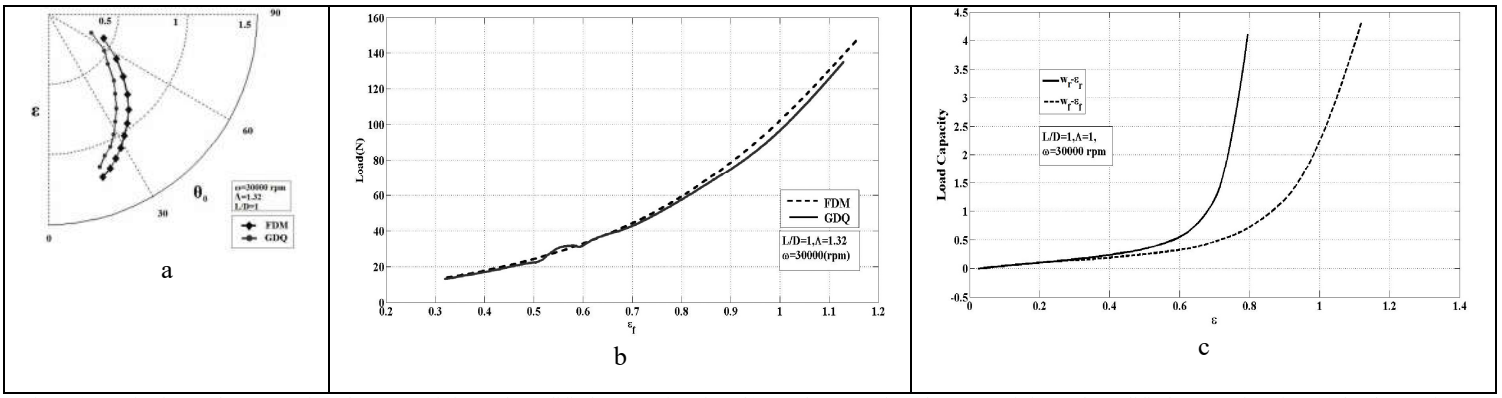

Fig. 5 (a) Attitude Angle Comparison between Finite and Modified Approximation (b) Load Comparison between Finite and Modified Approximation (c) load capacity for rigid and foil bearing

Fluid Film Thickness and Hydrodynamic Pressure

The optimum film profile is one that would result in the highest load carrying capacity. Shown in Fig. 9 is the film thickness for the bearing running at 30,000 rpm with assumed h_{min} of about 10.5 mm. The corresponding film thickness for a rigid bearing is also plotted for comparison. The steady-state eccentricity ratio of the foil bearing converged to 1.12 in this case. As shown in Figure 9, a foil bearing provides a more uniform profile in the vicinity of h_{min} than does the rigid bearing. Also, in a foil bearing the convergent region of the film gap spans over a greater area and the convergence is more pronounced than that of a rigid bearing due to the deformation of the foils under the hydrodynamic pressure.

Fig. 6(a) represents the film thickness profile between the FDM and GDQM at the mid-section of the bearing running at 30,000 rpm with an eccentricity ratio ε_r = 0.7 , L/D=1. Fig. 6 (b) represents the film thickness profile comparison between a rigid bearing and compliant bearing. The overall film profile for a foil bearing spans over a greater area due to the deformation of the foils.

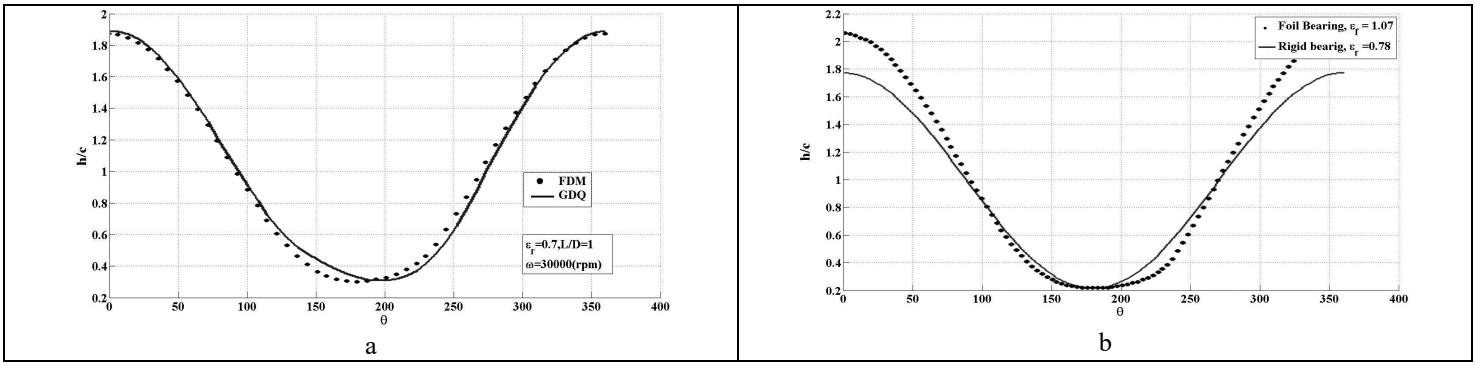

Fig. 6 (a) Film Thickness Profile Comparison between FDM & GDQM Approximation at 30,000 rpm (b) Film Thickness Comparison at Mid Section of Bearing at 30,000 rpm.

The reduction of the minimum film thickness resulting from the thin top foil is more dominant with a higher static load due to the excessive sagging of the top foil between bumps. This phenomenon is clearly shown in Fig. 7(a), which presents the top foil deflections, pressure distributions, and film thicknesses for various top foil thicknesses along the bearing midplane. As shown in the figure, a thin top foil leads to excessive sagging of the top foil between bumps, resulting in a reduction of the minimum film thickness. Therefore, too thin a top foil may decrease the load capacity of the foil bearing. Fig. 7(b) represents the pressure profile comparison between the FDM and GDQM at the mid-section of the bearing running at 30,000 rpm with an eccentricity ratio ε_r = 0.7. These profiles were obtained by varying the eccentricity ratio using the bisection method to match the minimum film thickness value at the given eccentricity ratio obtained by FDM. The program converged when the minimum film thickness of the bearing matched with the minimum film thickness obtained by FDM. Fig. 7(c) represents the pressure profile comparison between a rigid bearing and first-generation foil bearing whose properties are indicated in Table 2 (Peng, 2003). The operating speed is 30,000 rpm.
It is worth to point out that Fig. 8 represents the three-dimensional plot obtained by GDQM for a bearing running at 30,000 rpm and eccentricity ratio ε_r=0.7.

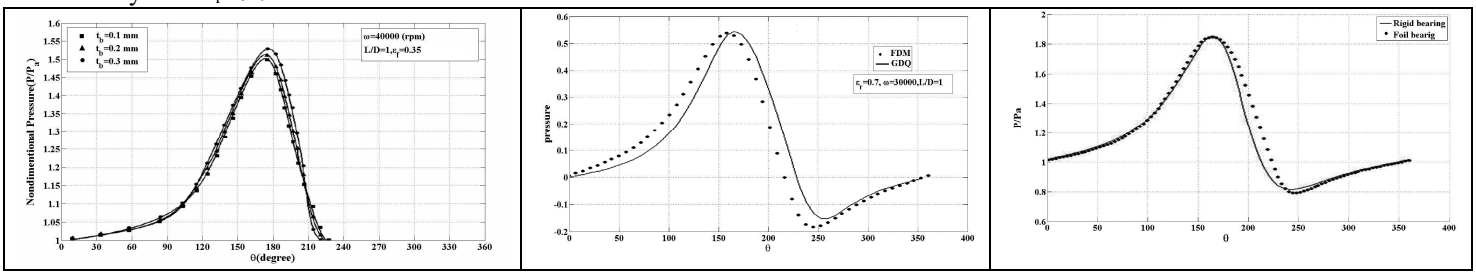

Fig. 7 (a) nondimensional Top foil deflection for various top foil thicknesses, t_f=0.05 mm, ω=40 krpm (b) Pressure Profile Comparison between Finite difference and generalized differential quadrature method at Mid Section of bearing at 30,000 rpm. (c) Pressure Profile Comparison at Mid Section of Bearing at 30,000 rpm

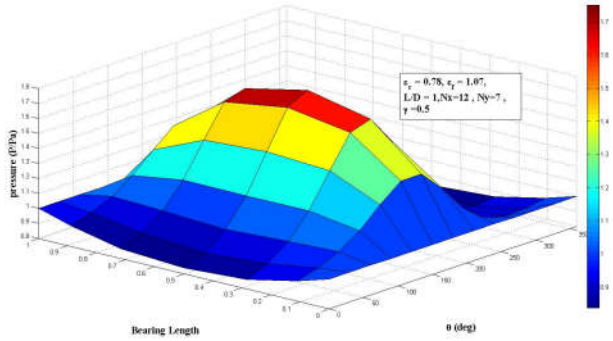

Fig. 8 Three Dimensional Pressure Distribution for Foil Bearing at 30,000 rpm based on GDQM.

References:

[1] M. Mehdizadeh, S. Akbarzadeh, K. Shams, and M. Khonsari, "Experimental investigation on the effect of operating conditions on the running-in behavior of lubricated elliptical contacts," *Tribology Letters,* vol. 59, no. 1, p. 6, 2015.

[2] A. Akbarzadeh, M. Mehdizadeh, S. Akbarzadeh, and K. Shams, "Effect of Nanoparticles on the Running-in Behavior in Lubricated Point Contact," *STLE, Dallas,* 2015.

[3] M. Mehdizadeh and S. Akbarzadeh, "Experimental investigation and a model to predict the steady-state friction coefficient in the lubricated contact," *STLE, Vegas,* 2016.

[4] H. Block, "The Foil Bearings-A New Departure in Hydrodynamic Lubrication," *Lubrication Engineering,* vol. 316, 1953.

[5] T. Emerson, "APPLICATION OF FOIL AIR BEARING TURBOMACHINERY IN AIRCRAFT ENVIRONMENTAL CONTROL SYSTEMS," 1978.

[6] H. Heshmat, W. Shapiro, and S. Gray, "Development of foil journal bearings for high load capacity and high speed whirl stability," *Journal of Lubrication Technology,* vol. 104, no. 2, pp. 149-156, 1982.

[7] J. Walowit, J. Anno, and B. Hamrock, "Modern developments in lubrication mechanics," ed: American Society of Mechanical Engineers, 1977.

[8] H. Heshmat, J. Walowit, and O. Pinkus, "Analysis of gas-lubricated foil journal bearings," *Journal of Lubrication Technology,* vol. 105, no. 4, pp. 647-655, 1983.

[9] H. Heshmat and C.-P. R. Ku, "Structural damping of self-acting compliant foil journal bearings," *Journal of tribology,* vol. 116, no. 1, pp. 76-82, 1994.
[10] H. Heshmat, "Advancements in the performance of aerodynamic foil journal bearings: high speed and load capability," *Journal of Tribology,* vol. 116, no. 2, pp. 287-294, 1994.
[11] A. Haghshenas and A. G. J. P. o. t. I. o. M. E. Arani, Part C: Journal of Mechanical Engineering Science, "Nonlocal vibration of a piezoelectric polymeric nanoplate carrying nanoparticle via Mindlin plate theory," vol. 228, no. 5, pp. 907-920, 2014.
[12] V. Mortezavi, A. Haghshenas, M. Khonsari, and B. J. I. J. o. F. Bollen, "Fatigue analysis of metals using damping parameter," vol. 91, pp. 124-135, 2016.
[13] A. Haghshenas and M. J. M. L. Khonsari, "Evaluation of fatigue performance of additively manufactured SS316 via internal damping," 2018.
[14] C. DellaCorte and M. J. Valco, "Load capacity estimation of foil air journal bearings for oil-free turbomachinery applications," *Tribology Transactions,* vol. 43, no. 4, pp. 795-801, 2000.
[15] Z.-C. Peng and M. Khonsari, "Hydrodynamic analysis of compliant foil bearings with compressible air flow," *Journal of tribology,* vol. 126, no. 3, pp. 542-546, 2004.
[16] A. H. Reddy, "Hydrodynamic Analysis of Compliant Journal Bearings," Louisiana State University, 2005.
[17] Z. Peng, "Thermohydrodynamic analysis of compressible gas flow in compliant foil bearings," 2003.
[18] M. Malik and C. Bert, "Differential quadrature solutions for steady-state incompressible and compressible lubrication problems," *Journal of Tribology,* vol. 116, no. 2, pp. 296-302, 1994.
[19] R. Bellman, *Methods of nonlinear analysis*. Elsevier, 1970.
[20] R. Hamming, *Numerical methods for scientists and engineers*. Courier Corporation, 2012.
[21] S. Rohde and K. Oh, "Higher order finite element methods for the solution of compressible porous bearing problems," *International Journal for Numerical Methods in Engineering,* vol. 9, no. 4, pp. 903-911, 1975.
[22] A. Z. Szeri, *Tribology: friction, lubrication, and wear*. McGraw-Hill, 1980.

KEYWORDS
Gas Foil Journal Bearing; Gas Rigid Journal Bearing; Hydrodynamic Pressure; Generalized Differential Quadrature Method.